Title
Intravascular innate immune cells reprogrammed via intravenous nanoparticles to promote functional recovery after spinal cord injury

Journal
Proceedings of the National Academy of Sciences of the United States of America, 116(30)

ISSN
0027-8424

Authors
Park, Jonghyuck
Zhang, Yining
Saito, Eiji
et al.

Publication Date
2019-07-23

DOI
10.1073/pnas.1820276116

Classification: BIOLOGICAL SCIENCES: Applied Biological Sciences

Intravascular innate immune cells reprogrammed via intravenous nanoparticles to promote functional recovery after spinal cord injury

Jonghyuck Park[1], Yining Zhang[2], Eiji Saito[1], Brian J. Cummings[3,4], Aileen J. Anderson[3,4], and Lonnie D. Shea[1,2]*

[1]Department of Biomedical Engineering, University of Michigan, Ann Arbor, MI 48105
[2]Department of Chemical Engineering, University of Michigan, Ann Arbor, MI 48105
[3]Department of Anatomy and Neurobiology, University of California, Irvine, CA 92697
[4]Department of Physical Medicine and Rehabilitation, University of California, Irvine, CA 92697

*Address Correspondence to:

Dr. Lonnie D. Shea
University of Michigan
Department of Biomedical Engineering
2200 Bonisteel Blvd
1119 Carl A. Gerstacker Building
Ann Arbor, MI 48109-2099
Phone: 734-764-7149
E-mail: ldshea@umich.edu

Abstract

Traumatic primary spinal cord injury (SCI) results in paralysis below the level of injury and is associated with infiltration of hematogenous innate immune cells into the injured cord. Methylprednisolone has been applied to reduce inflammation following SCI, yet was discontinued due to an unfavorable risk-benefit ratio associated with off-target effects. In this study, intravenously administered poly(lactide-co-glycolide) nanoparticles were internalized by circulating monocytes and neutrophils, reprogramming these cells based on their physicochemical properties and not an active pharmaceutical ingredient, to exhibit altered biodistribution, gene expression, and function. Nanoparticle positive immune cells were observed within the injury, and additionally, the overall accumulation of innate immune cells at the injury was reduced, coinciding with downregulated expression of pro-inflammatory factors and increased expression of anti-inflammatory and pro-regenerative genes. Furthermore, nanoparticle administration induced macrophage polarization towards pro-regenerative phenotypes at the injury and markedly reduced both fibrotic and gliotic scarring. Moreover, nanoparticle administration with the implanted multichannel bridge led to increased numbers of regenerating axons, increased myelination, and an enhancement in locomotor function synergistically after SCI. These data demonstrate that nanoparticles provide a platform that limits acute inflammation and tissue destruction, at a favorable risk-benefit ratio, leading to a pro-regenerative microenvironment that supports regeneration and functional recovery. These particles may have applications to trauma and potentially other inflammatory diseases.

Significance Statement

Inflammatory responses, such as those following spinal cord injury (SCI), lead to extensive tissue damage that impairs function. Here, we present nanoparticles that target circulating immune cells acutely, with nanoparticles reprogramming the immune cell response. The polymeric nanoparticles are formed without an active pharmaceutical ingredient that can have off-target effects, and internalization redirects some immune cells to the spleen, with modest numbers at the SCI. Following intravenous delivery, immune cell infiltration is reduced, correlating with decreased tissue degeneration. Furthermore, the SCI develops into a permissive microenvironment characterized by pro-regenerative immune cell phenotypes, expression of regeneration associated genes, increased axons and myelination, and a substantially improved functional recovery. These nanoparticles may have application to numerous inflammatory diseases.

Keywords

Spinal cord injury, nerve regeneration, nanomedicine, immunoengineering

Introduction

Traumatic spinal cord injury (SCI) results in an initial injury, followed by secondary events that can last from hours to weeks leading to permanent loss of function (1-3). Inflammatory responses are initiated in part by the rapid influx of immune cells, including inflammatory monocytes and neutrophils, via a broken blood-spinal cord barrier (BSCB). These cells infiltrate the injury site within hours and secrete pro-inflammatory cytokines, reactive oxygen species (ROS), and nitric oxide (NO), all of which can contribute to additional neuronal cell death, axonal demyelination, and functional deficits following SCI (4-6). Critically, while glucocorticoids such as methylprednisolone were once the standard of care for acute SCI due to their anti-inflammatory properties, these agents are also associated with unfavorable side effects, such as sepsis, gastrointestinal bleeding, and thromboembolism (7), indicating that improved methods are needed. Systemic depletion of neutrophils or monocytes has either not altered or a small effect on SCI outcome (8, 9). Because monocytes and neutrophils are necessary for would healing and tissue regeneration after injury, reprogramming the immune response could be a more effective strategy to minimize loss of function and enable repair.

We have previously demonstrated that 500 nm diameter poly(lactide-co-glycolide) (PLG)-based nanoparticles (NPs) carrying a negative zeta potential distracts circulating immune cells such as inflammatory monocytes and neutrophils away from the injury site (10, 11). Intravenously administered NPs reduced pathological symptoms and produced a therapeutic benefit in inflammation-medicated diseases on central nervous system (CNS) including West Nile virus (WNV) encephalitis and experimental autoimmune encephalomyelitis (EAE) (10-12). Highly negatively charged NPs are thought to bind to the scavenger receptor on circulating immune cells, effectively reprogramming them to influence their trafficking to the spleen, and thus indirectly attenuate the immune pathology at the inflamed area (11, 12). In SCI, recent studies demonstrate that hematogenous-infiltrating immune cells are predominantly responsible for secondary axonal dieback, suggesting that reducing hematogenous immune cells infiltration at early time point may indirectly reduce tissue degeneration by attenuating the inflammation-mediated secondary events (5, 13). Reprogramming immune cells to accumulate at the injury and assume pro-regenerative phenotypes may provide a means to directly modulate the injury environment to promote regeneration.

Herein, we investigate NPs that reprogram inflammatory cells intravascularly to obtain a fraction that home to the injury and modulate the microenvironment, resulting in enhanced regeneration and functional recovery after SCI. NPs (500 nm diameter, zeta potential < -30 mV) were administered intravenously daily for 7 days immediately after SCI. A lateral hemisection SCI model was employed, with bridge implantation employed in all studies as a means to define a region in which spared axons can be distinguished from regenerating axons (SI appendix, Fig. S1). We investigate the biodistribution of NPs among tissues by fluorescence imaging, and subsequently within the spinal cord. Inflammatory responses were characterized histologically and through gene expression analysis. Regeneration following NPs treatment was assessed through the number of axons, the presence of serotonergic axons, and myelination of axons, with locomotor functional testing performed. The administration of NPs that targets innate immune cells to reprogram their function represents a novel strategy for neuroprotection and neuroregeneration after SCI.

Results

Nanoparticles internalization and inflammatory monocytes sequestration.

In vivo images were acquired to investigate the biodistribution of NPs. Initially, NPs (1 mg, Cy5.5-conjugated (NPs-Cy5.5)) were administered intravenously on a daily basis for 7 days starting the day of injury (Fig. 1A). The spinal cord and spleen were collected for analysis at day 1, 4, and 8 post-injection from all conditions (day 7, 10, and 14 post-SCI) (Fig.1B and SI appendix, Fig. S2). In both SCI and sham groups, the greatest fluorescence intensity from NPs was observed in spleen (Fig.1B and 1C). However, fluorescence associated with NPs was also observed in the spinal cord in the SCI group. Radiant efficiency levels associated with NPs-Cy5.5 in the spinal cord were approximately three-fold greater in the SCI group compared to the sham group; in contrast, in the spleen, no differences were observed between sham and SCI groups. Subsequently, fluorescence levels gradually decreased in both sites over time (SI appendix, Fig. S2). At day 4 post-injection (day 10 post-SCI), the fluorescence associated with NPs-Cy5.5 was substantially decreased in the spleen, yet no significant differences were observed in the spinal cord compared to those at day 1 post-injection. However, the fluorescence associated with NPs-Cy5.5 was decreased in all organs as in naïve group at day 8 post-injection (SI appendix, Fig. S2B and S2C).

Next, the distribution of particles within the spinal cord and cell types with internalized particles were investigated. Cy5.5 fluorescence was observed within the bridge area after SCI (Fig. 1D). In addition, immunofluorescence data indicated that about 80% of NPs-Cy5.5 were colocalized with 7/4 $(Ly\text{-}6B.2)^{+}$ inflammatory monocytes/neutrophils within the bridge (Fig. 1E-1G). Anti-7/4 was selected as a marker for inflammatory monocytes/neutrophils, since the 7/4 antigen is present on the cell surface of both inflammatory monocytes and neutrophils (14, 15). We subsequently investigated inflammation within the spinal cord, specifically focusing on the accumulation of inflammatory monocytes/neutrophils and gene expression associated with immune cells. At days 7 and 10 post-SCI, $7/4^{+}$ cell numbers in the injury with NPs administration were significantly reduced relative to control conditions (Fig. 1H and 1I). Gene expression levels for neutrophils (CD11b and Ly6G) and inflammatory monocytes (CCR2 and Ly6C) were investigated in the spinal cord and spleen at day 7 post-SCI. The data indicated that NPs administration significantly decreased the expression of genes associated with neutrophils and inflammatory monocytes within the spinal cord compared to the PBS group (SI appendix, Fig. S3A). Although Ly6C gene expression level within the spleen for NPs treatment trended toward greater expression compared to the PBS group, these trends were not significant. However, CD11b, Ly6G, and CCR2 expression levels in the spleen from the NPs group were significantly increased relative to the PBS group (SI appendix, Fig. S3B). Collectively, in agreement with previous studies (11, 12), these results suggest that NPs administration associates with innate immune cells such as inflammatory monocytes and neutrophils, which influence their numbers in the spleen and spinal cord. In addition, NPs administration contributes to decreasing immune cells accumulation at inflamed sites.

Nanoparticles induce macrophages polarization at the injury site

We next investigated macrophage polarization following NPs treatment of SCI, as macrophages play pivotal roles in inflammatory responses after injury (5, 16) (Fig. 2). Macrophages have the potential for plasticity in their phenotype depending on their

microenvironment, and although macrophage phenotypes are not binary, they have been classified as inflammatory M1 and pro-regenerative M2 phenotypes for ease of description (16). We have reported that M2 macrophages contribute to creating pro-regenerative microenvironments leading to axonal regrowth and remyelination, and locomotor recovery after SCI (17, 18). Analysis of markers for M1 and M2 macrophages in the spinal cord indicated that expression levels of the pro-inflammatory markers inducible nitric oxide synthase (iNOS), CD86, and monocyte chemoattractant protein-1 (MCP-1) were significantly downregulated in the NPs compared to the PBS group from day 7. As key markers for M1 phenotypes, these factors are associated with inflammatory responses and release of pro-inflammatory factors, contributing to an inhibitory microenvironment at the injury (16). In contrast, levels of the M2 markers CD206 and interleukin (IL)-10 were significantly increased in the NPs relative to the PBS group. These results were maintained until day 84 post-SCI (Fig. 2A-B). In agreement with previous studies (17, 19), no difference was observed in Arginase1 (Arg1) expression between groups at day 7, yet Arg1 was significantly upregulated following NPs treatment at day 14 and 84 post-SCI compared to PBS. Interestingly, expression levels of pro-inflammatory factors (CD86 and MCP-1) were reduced in the PBS group compared to SCI only, while anti-inflammatory markers (Arg1 and CD206) were substantially increased in the PBS group compared to SCI only at day 84 post-SCI, indicating a role of the bridge for limiting inflammation. Subsequently, immunofluorescence data was investigated to quantify the total number of $CD206^+$ cells ($Hoechst^+/CD206^+$), macrophages ($Hoechst^+/F4/80^+$), and M2 macrophages ($Hoechst^+/F4/80^+/CD206^+$) at day 7 and 84 post-SCI (Fig. 2C and 2D). The number of $CD206^+$ cells was significantly increased in the NPs compared to PBS group (Fig. 2F). The density of pro-regenerative M2 macrophages was also upregulated for NPs group at day 7 and 84 post-SCI (Fig. 2G). Furthermore, no statistical difference was noted in the total number of infiltrated macrophages for all conditions (Fig. 2E) over time, thus the ratio of M2 phenotypes to the total number of macrophages was substantially upregulated in NPs group (Fig. 2H). Therefore, NPs administration influences macrophage polarization at the SCI.

Nanoparticles treatment decreases scarring formation after SCI

SCI results in formation of both fibrotic and gliotic scar tissues at the lesion epicenter, we therefore investigated the impact of the NPs on these parameters. The scar tissue acts as a mechanical barrier to axon elongation and inhibiting axonal regeneration through accumulation of inhibitory molecules as a chemical barrier (1, 2). A fibrotic scar is characterized by accumulation of fibronectin, fibroblasts, and various extracellular matrix (ECM) molecules (20). Reactive astrocytes play prominent roles in formation of gliotic scar and act as a major impediment to axonal regeneration (2). At 4 weeks post-SCI, the area of fibrotic scar tissue in the NPs treatment group was significantly decreased compared to PBS (Fig. 3A and 3B). Similar to the level of fibronectin, the area of glial fibrillary acidic protein (GFAP) staining in the NPs group was also substantially decreased relative to the PBS group (Fig. 3C and 3D). These data indicate that NPs administration significantly decreased both fibrotic and gliotic scarring after SCI.

Nanoparticles enhance axonal regrowth and remyelination within an implanted PLG bridge

We investigated the impact of NPs treatment on axonal regrowth and myelination in the chronic (day 84 post-SCI) phase of SCI (Fig. 4). Spinal cord sections were stained using neurofilament 200 (NF200), myelin basic protein (MBP), and myelin protein zero (P0). Immunofluorescence data indicated that axons were observed throughout the bridges in all conditions (Fig. 4A and 4B). High magnification images showed that regenerating axons were

found in bundles within the bridge (Fig. 4A' and 4B'). NPs administration substantially increased the number of $NF200^+$ axons relative to the PBS group (Fig. 4C). Similar to $NF200^+$ axons number, all myelinated axons ($NF200^+/MBP^+$) were increased 3-fold in response to NPs relative to PBS injection. In addition, the significantly greater number of oligodendrocyte- ($NF200^+/MBP^+/P0^-$) and Schwann cell-derived myelinated ($NF200^+/MBP^+/P0^+$) axons were observed for NPs treatment relative to the PBS group. Furthermore, about 43% of the $NF200^+$ axons were myelinated in the NPs condition, with approximately 40% of those axons myelinated by oligodendrocytes. Collectively, these data suggest that NPs produce an environment more permissive to axonal growth and remyelination after SCI.

Nanoparticles increase the density of serotonergic fibers after SCI

The presence of axons that are positive for the neurotransmitter serotonin (or 5-HT) was assessed because these axons have been associated with recovery of function and attenuation of allodynia/hyperalgesia after SCI (21, 22). This role of 5-HT axons in function makes it a good marker for regeneration of descending tracts. Spinal cord tissues were immunostained for 5-HT at day 84 post-SCI, and the densities of 5-HT fibers quantified at three distinct locations of the bridge: rostral, central, and caudal (Fig. 5 and SI appendix, Fig. S1C). 5-HT-fibers were identified throughout the bridge (Fig. 5A and 5B), however, a greater number of 5-HT fibers was observed with NPs treatment in all three locations compared to PBS (Fig. 5A', 5B' and 5C). These data suggest that in addition to the observation of neurofilament axons and active remyelination within the bridge, NPs treatment specifically resulted in the growth of descending motor axons as assessed by density of 5-HT fibers within the bridge.

Nanoparticles improve locomotor function after SCI

We next investigated the expression of regeneration-associated genes (RAGs) following NPs administration in the acute and chronic SCI phase from the injured spinal cord tissue (Fig. 6A and 6B). Genes were selected from neural system development (Gene ontology (GO) accession number; GO:0007399), locomotor recovery-(GO:0007626), and chemical synaptic transmission-(GO:0007268) associated gene ontologies based on a previous study (18). Gene expression data indicated that selected genes had upregulated expression in the NPs group for both the acute and chronic phase of SCI relative to PBS injection. Interestingly, in the chronic SCI phase, expression levels of RAGs (ChAT, Hoxd10, and Lhx5) in PBS injection group were also statistically upregulated relative to SCI only group, suggesting a role for the bridge alone in supporting regeneration. Subsequently, ipsilateral hindlimb locomotor recovery was assessed through the Basso Mouse Scale (BMS) before injury, at day 3, and weekly for 84 days after SCI (Fig. 6C). All animals exhibited normal open field locomotion before SCI (BMS;9). No ipsilateral hindlimb movement was observed at day 3 post-SCI in any treatment group (BMS;0). However, BMS scoring in the NPs group revealed a substantially improved locomotor function compared to PBS group from day 7 through day 84 after SCI. In agreement with gene expression data, the BMS score in PBS group was significantly increased relative to SCI only group from day 70 post-SCI, indicating that the bridge itself also has a positive effect on locomotor recovery. These data demonstrate that NPs have an early effect on reprogramming of circulating immune cells, which synergize with the microenvironment created by the bridge to induce long-term expression of RAGs at the injury, resulting in a pro-regenerative microenvironment that is associated with an improved locomotor function after SCI.

Discussion

In the present study, we investigated the potential for reprogramming of circulating innate immune cells through NPs administration to enhance functional regeneration following SCI. The rapid infiltration of various immune cells such as inflammatory monocytes and neutrophils into the SCI leads to inflammatory response-derived secondary damage, contributing to further neuronal cell death, axonal dieback, demyelination, and scar tissue formation (4, 23). For in vivo SCI treatment, systemic depletion of immune cells has led to mixed results with some studies showing improved regeneration with partial depletion of select immune populations (24), while other studies show worsened histological and functional outcomes with complete depletion of certain immune populations (23, 25). Herein, we focused on a non-depleting strategy targeting inflammatory cells in the vasculature, prior to their extravasation to the injury. We tested the hypothesis that particles could reprogram innate immune cell trafficking and phenotype to limit deleterious inflammatory responses, and promoting an environment that is a more permissive for regeneration.

Intravenously delivered NPs influence trafficking patterns of inflammatory monocytes and neutrophils, with a modest proportion of NPs-positive cells trafficking to the spinal cord and the majority accumulating in the spleen. Intravenously administered NPs are thought to bind to circulating immune cells via scavenger receptors such as MARCO. Previous studies reported that neither resident microglia or T lymphocytes express scavenger receptors such as MARCO (26), thus indicating NPs target selectively circulating immune cells that would normally infiltrate a SCI. The sequestration of inflammatory monocytes/neutrophils in the spleen has been observed in other inflammation-mediated diseases models by NPs treatment (11-13). In agreement with these previous studies, NPs reduced the number of inflammatory monocytes/neutrophils in the injured spinal cord (Fig. 1E-1I), with this decrease likely indirectly decreasing tissue degeneration due to the reduced immune cell infiltration. However, we observed that NPs-positive cells were present within the spinal cord, and our data suggest that these cells directly influenced the microenvironment by inducing a pro-regenerative phenotype that was more permissive for tissue regeneration. These results are also supported by gene expression analysis (SI appendix Fig. S3). In particular, both human and mice inflammatory monocytes express CCR2, which is principally responsible for recruitment and accumulation of these cells at inflammatory sites (11, 27). Previous study showed that delivery of CCR2 small interfering RNAs (siRNAs) via liposome reduced inflammatory monocyte trafficking in inflammatory disease models (27). However, because of widespread expression of CCR2 in other immune cells such as B cells and T cells, targeting CCR2 may have undesired side effects (28, 29).

The cumulative effect of NPs treatment is modulation of the microenvironment, which induces macrophage polarization from a pro-inflammatory phenotype towards a pro-regenerative phenotype. In the intact CNS, microglia/macrophages have both M1 and M2 properties, however, following SCI, pro-regenerative M2 macrophages are typically decreased, while pathological M1 phenotypes are increased and produce pro-inflammatory factors (19). Therefore, a transient and low number of M2 phenotype cells at the injury may fail to control secondary inflammatory events following primary SCI. NPs treatment modulated the microenvironment and led to an M2-enhanced environment at the SCI site, with downregulation of pro-inflammatory factors and upregulated expression of anti-inflammatory factors such as Arg1, CD206, and IL-10 throughout day 84 post-SCI. Interestingly, NPs treatment also decreased the expression level of MCP-1, which is responsible for attracting circulating inflammatory monocytes to injuries by binding to its receptor CCR2 (11) and may also influence trafficking patterns of inflammatory monocytes after

SCI. In addition, downregulation of pro-inflammatory factors following NPs treatment indicates that repeated-administration of NPs was well tolerated and reduced scar formation. Arg1 has been shown to promote wound healing and decrease the intensity and duration of inflammation (18). Similarly, CD206 and IL-10 both have demonstrated roles in modulating immune responses and secondary damage after injury. CD206 binds and removes apoptotic and necrotic cells without generation of cytotoxic byproducts after injury (19). The anti-inflammatory cytokine IL-10 suppresses nuclear factor-κB (NF-κB) activation, leading to downregulation of pro-inflammatory factors secretion (18). Consistent with these roles, NPs treatment upregulated the number of $CD206^+$ cells and M2 macrophages ($CD206^+/F4/80^+$) compared to the PBS group.

NPs treatment significantly reduced both fibrotic and gliotic scarring after SCI. Lesion scarring represents both a mechanical and chemical impediment to axonal outgrowth and regeneration, and previous studies have demonstrated that macrophages lead to a pro-fibrotic microenvironment by releasing pro-inflammatory factors. In both mice and human, these pro-inflammatory factors contribute to fibroblast activation and the induced secretion of connective tissue growth factor (CTGF) and collagen IV through SAMD2/3-mediated pathways, initiating formation of a dense, insoluble fibrotic matrix (30, 31). Additionally, prior reports demonstrate that both circulating immune cells and hematogenous-derived macrophages recruit perivascular fibroblasts at the SCI, while depleting of hematogenous macrophages decreases the fibroblast accumulation and fibrotic scar area, enhancing axonal regrowth (32). In addition to fibrotic scarring, astrocytes also become reactive after SCI and are major component of gliotic scarring. Reactive astrocytic responses are also initiated by pro-inflammatory factors that act through upregulation of extracellular signal regulated kinase (ERK) signaling (7). In this study, NPs inhibition of immune cell accumulation, induction of pro-regenerative phenotypes, and generation of anti-inflammatory factors at the injury site may have altered fibroblast migration and astrocyte activation, reducing fibrotic and gliotic scarring and promoting axonal regeneration following SCI.

NPs treatment has positive effects on axonal regeneration and remyelination after SCI. In the inflammatory microenvironment, pro-inflammatory factors are cytotoxic to neuronal cells and stimulate a short and arborizing growth pattern of axons after SCI (7, 19, 33). NPs administration promotes axonal regrowth throughout the implanted-multichannel bridges compared to PBS injection. In the data reported herein, NPs treatment influences the gene expression dynamics and macrophages polarization at the injury. Increased Arg1 by NPs at the injury enhances overexpression of polyamines, promoting cAMP downstream signaling pathway to activate axonal regrowth even in a myelin inhibitory microenvironment (19). IL-10 has been reported to upregulate expression of anti-apoptotic factors and provide a direct trophic effect on axonal regeneration under the neurotoxic microenvironment (18). CD206 promotes tissue remodeling after injury involving wound retraction and inflammatory resolution for tissue homeostasis (5). All of these factors may contribute to creating a pro-regenerative environment after SCI leading to axonal regeneration. Axonal remyelination after SCI is considered as a major component of the regenerative process and is mediated by multipotent oligodendrocytes progenitor cells (OPCs). Previous studies have indicated that macrophages polarization into pro-regenerative M2 phenotypes is an essential step for differentiation of OPCs for remyelination after SCI (34). Moreover, an M2 mediated-regenerative factor activin-A directly binds to OPCs and facilitate OPCs differentiation at the SCI (35). Therefore, NPs treatment-mediated reprogramming of innate immune cells towards pro-regenerative phenotypes may be a key component of the regenerative process for axonal regeneration and remyelination after SCI.

The early effects of NPs treatment synergize with multichannel bridge to upregulate long-term expression of RAGs and enhance functional recovery after SCI. Previously, we reported that bridge implantation alone increased the expression levels of axonal guidance- and synaptogenesis-associated gene ontologies at the SCI lesion (18), and altered the chemical balance and physical cues for a more permissive environment, leading to injury stabilization and attenuation of inflammatory responses (7, 17, 18). Furthermore, mechanical guidance by the 3D structure of the bridge contributed to regeneration of descending axons and an increase in growth associated protein 43 (GAP-43) expression below the injury site, leading to forelimb functional recovery (36). These characteristics of bridge implantation are consistent with the observed upregulation of RAGs expression and reduction of pro-inflammatory factors in our control group, which consisted of PBS injections in conjunction with bridge implantation. BMS scores in the NPs group were significantly increased starting from 1-week post-SCI compared to PBS, indicating that rapid NPs-mediated inhibition of inflammatory immune cells accumulation led to less degeneration for rapid recovery of motor function. Furthermore, an improvement of locomotor skills was also observed from the PBS group at the chronic SCI phase compared to SCI only, which likely results from a more permissive environment enabling regeneration. These results were also supported by gene expression data. NPs-derived immune cells modulation led to the long-term expression of multiple anti-inflammatory factors and RAGs and induced a pro-regenerative environment at the injury. A number of genes associated with motor neurons were observed to be upregulated at later time points. Choline acetyltranferase (ChAT), which marks mature motor neurons (37), had increased expression. Similarly, an increased expression of Homeobox D10 (Hoxd10) was observed, which organizes the patterning of motor neurons in the spinal cord (38). LIM homeobox 5 (Lhx5), implicated in the proliferation and differentiation of motor neurons (39), and transient receptor potential channel subfamily C (Trpc5), which leads to differentiation of neural progenitor cells (40), were also upregulated. Following SCI, descending serotonergic projections to spinal motor neurons were disrupted, leading to a decrease in serotonin levels and enhancing the locomotor dysfunction (21, 22). Our data demonstrates that NPs treatment upregulates the number of 5-HT fibers within bridges, which also may contribute to locomotor recovery. Taken together, these data demonstrate that NPs treatment has early and rapid therapeutic impacts which have long term consequences with multichannel bridges synergistically, contributing to immune cells reprogramming towards pro-regenerative phenotypes. In addition, these effects lead to the long-term upregulation of anti-inflammatory factors, RAGs and serotonergic fibers, promoting locomotor recovery after SCI.

In conclusion, this report demonstrates that NPs treatment can modulate the inflammatory microenvironment after SCI. NPs-mediated rapid reprogramming of innate immune cells has a sustained impact on microenvironment modulation at the SCI injury when combined with bridge implantation. In addition, this regenerative microenvironment initiates a cascade of events, including induction of gene expression profiles associated with neural development and regeneration, which likely contributes to the enhanced numbers of regenerating and myelinated axons and improved functional recovery. Collectively, this strategy of targeting the innate immune cells in the vasculature prior to their extravasation to a SCI may have applications to other injury models associated with inflammation-mediated tissue damage. Furthermore, NPs are made of an FDA-approved material, stable at room temperature, do not contain an active pharmaceutical ingredient (API), and can be readily stored for immediate intravenous administration within the standard of therapy guidelines to limit secondary damage.

Materials and Methods

For additional methods, see SI Appendix.

Multichannel bridges fabrication

Using a gas foaming and particulate leaching method, multichannel bridges were fabricated.

Nanoparticle fabrication and injection

Cyanine 5.5 amine dye conjugated Poly(D,L-lactide-co-glycolide) based particles were fabricated using an oil-in-water single emulsion solvent evaporation method. Each animal received 1 mg of particles (200 μl of suspension) via tail veil injection within two hours after SCI per day for 7 days.

Animals

All animal surgery procedures and animal care were performed according to the Animal Care and use Committee guideline at University of Michigan. C57/BL6 female mice (6-8 weeks old, 20-25g; The Jackson Laboratory, Bar Harbor, ME, USA) were used to create hemisection SCI model.

Acknowledgements

This study was supported by the National Institute of Health (R01EB005678). Authors thank Unit for laboratory Animal Medicine at University of Michigan for animal care and maintenance.

1. Silver J & Miller JH (2004) Regeneration beyond the glial scar. *Nat Rev Neurosci* 5(2):146-156.
2. Yiu G & He Z (2006) Glial inhibition of CNS axon regeneration. *Nat Rev Neurosci* 7(8):617-627.
3. Park J*, et al.* (2010) Nerve regeneration following spinal cord injury using matrix metalloproteinase-sensitive, hyaluronic acid-based biomimetic hydrogel scaffold containing brain-derived neurotrophic factor. *J Biomed Mater Res A* 93(3):1091-1099.
4. Donnelly DJ & Popovich PG (2008) Inflammation and its role in neuroprotection, axonal regeneration and functional recovery after spinal cord injury. *Exp Neurol* 209(2):378-388.
5. Gensel JC & Zhang B (2015) Macrophage activation and its role in repair and pathology after spinal cord injury. *Brain Res* 1619:1-11.
6. Due MR*, et al.* (2014) Acrolein involvement in sensory and behavioral hypersensitivity following spinal cord injury in the rat. *J Neurochem* 128(5):776-786.
7. Park J*, et al.* (2018) Reducing inflammation through delivery of lentivirus encoding for anti-inflammatory cytokines attenuates neuropathic pain after spinal cord injury. *J Control Release* 290:88-101.
8. Wang J (2018) Neutrophils in tissue injury and repair. *Cell Tissue Res* 371(3):531-539.
9. Wilgus TA, Roy S, & McDaniel JC (2013) Neutrophils and Wound Repair: Positive Actions and Negative Reactions. *Adv Wound Care (New Rochelle)* 2(7):379-388.
10. Getts DR*, et al.* (2012) Microparticles bearing encephalitogenic peptides induce T-cell tolerance and ameliorate experimental autoimmune encephalomyelitis. *Nat Biotechnol* 30(12):1217-1224.
11. Getts DR*, et al.* (2014) Therapeutic inflammatory monocyte modulation using immune-modifying microparticles. *Sci Transl Med* 6(219):219ra217.
12. Getts DR, Shea LD, Miller SD, & King NJ (2015) Harnessing nanoparticles for immune modulation. *Trends Immunol* 36(7):419-427.
13. Jeong SJ*, et al.* (2017) Intravenous immune-modifying nanoparticles as a therapy for spinal cord injury in mice. *Neurobiology of Disease* 108:73-82.
14. Pineau I, Sun L, Bastien D, & Lacroix S (2010) Astrocytes initiate inflammation in the injured mouse spinal cord by promoting the entry of neutrophils and inflammatory monocytes in an IL-1 receptor/MyD88-dependent fashion. *Brain Behav Immun* 24(4):540-553.
15. Tsou CL*, et al.* (2007) Critical roles for CCR2 and MCP-3 in monocyte mobilization from bone marrow and recruitment to inflammatory sites. *J Clin Invest* 117(4):902-909.
16. David S & Kroner A (2011) Repertoire of microglial and macrophage responses after spinal cord injury. *Nat Rev Neurosci* 12(7):388-399.
17. Margul DJ*, et al.* (2016) Reducing neuroinflammation by delivery of IL-10 encoding lentivirus from multiple-channel bridges. *Bioeng Transl Med* 1(2):136-148.
18. Park J*, et al.* (2018) Local Immunomodulation with Anti-inflammatory Cytokine-Encoding Lentivirus Enhances Functional Recovery after Spinal Cord Injury. *Mol Ther* 26(7):1756-1770.
19. Kigerl KA*, et al.* (2009) Identification of two distinct macrophage subsets with divergent effects causing either neurotoxicity or regeneration in the injured mouse spinal cord. *J Neurosci* 29(43):13435-13444.
20. Soderblom C*, et al.* (2013) Perivascular fibroblasts form the fibrotic scar after contusive spinal cord injury. *J Neurosci* 33(34):13882-13887.
21. Ghosh M & Pearse DD (2014) The role of the serotonergic system in locomotor recovery after spinal cord injury. *Front Neural Circuits* 8:151.
22. Schmidt BJ & Jordan LM (2000) The role of serotonin in reflex modulation and locomotor rhythm production in the mammalian spinal cord. *Brain Res Bull* 53(5):689-710.
23. David S, Lopez-Vales R, & Wee Yong V (2012) Harmful and beneficial effects of inflammation after spinal cord injury: potential therapeutic implications. *Handb Clin Neurol* 109:485-502.

24. Popovich PG*, et al.* (1999) Depletion of hematogenous macrophages promotes partial hindlimb recovery and neuroanatomical repair after experimental spinal cord injury. *Exp Neurol* 158(2):351-365.
25. Stirling DP, Liu SH, Kubes P, & Yong VW (2009) Depletion of Ly6G/Gr-1 Leukocytes after Spinal Cord Injury in Mice Alters Wound Healing and Worsens Neurological Outcome. *Journal of Neuroscience* 29(3):753-764.
26. Hickman SE*, et al.* (2013) The microglial sensome revealed by direct RNA sequencing. *Nat Neurosci* 16(12):1896-1905.
27. Leuschner F*, et al.* (2011) Therapeutic siRNA silencing in inflammatory monocytes in mice. *Nat Biotechnol* 29(11):1005-1010.
28. Boros P, Ochando JC, Chen SH, & Bromberg JS (2010) Myeloid-derived suppressor cells: natural regulators for transplant tolerance. *Hum Immunol* 71(11):1061-1066.
29. Shantsila E*, et al.* (2011) Immunophenotypic characterization of human monocyte subsets: possible implications for cardiovascular disease pathophysiology. *J Thromb Haemost* 9(5):1056-1066.
30. Wynn TA & Barron L (2010) Macrophages: master regulators of inflammation and fibrosis. *Semin Liver Dis* 30(3):245-257.
31. Leask A & Abraham DJ (2004) TGF-beta signaling and the fibrotic response. *FASEB J* 18(7):816-827.
32. Zhu Y*, et al.* (2015) Hematogenous macrophage depletion reduces the fibrotic scar and increases axonal growth after spinal cord injury. *Neurobiol Dis* 74:114-125.
33. Park J*, et al.* (2014) Neuroprotective role of hydralazine in rat spinal cord injury-attenuation of acrolein-mediated damage. *J Neurochem* 129(2):339-349.
34. Miron VE*, et al.* (2013) M2 microglia and macrophages drive oligodendrocyte differentiation during CNS remyelination. *Nat Neurosci* 16(9):1211-1218.
35. de Kretser DM, O'Hehir RE, Hardy CL, & Hedger MP (2012) The roles of activin A and its binding protein, follistatin, in inflammation and tissue repair. *Mol Cell Endocrinol* 359(1-2):101-106.
36. Pawar K*, et al.* (2015) Biomaterial bridges enable regeneration and re-entry of corticospinal tract axons into the caudal spinal cord after SCI: Association with recovery of forelimb function. *Biomaterials* 65:1-12.
37. Yuan Q, Su H, Chiu K, Lin ZX, & Wu W (2014) Assessment of the rate of spinal motor axon regeneration by choline acetyltransferase immunohistochemistry following sciatic nerve crush injury in mice. *J Neurosurg* 120(2):502-508.
38. Lin AW & Carpenter EM (2003) Hoxa10 and Hoxd10 coordinately regulate lumbar motor neuron patterning. *J Neurobiol* 56(4):328-337.
39. Paylor R, Zhao Y, Libbey M, Westphal H, & Crawley JN (2001) Learning impairments and motor dysfunctions in adult Lhx5-deficient mice displaying hippocampal disorganization. *Physiol Behav* 73(5):781-792.
40. Shin HY*, et al.* (2010) A role of canonical transient receptor potential 5 channel in neuronal differentiation from A2B5 neural progenitor cells. *PLoS One* 5(5):e10359.

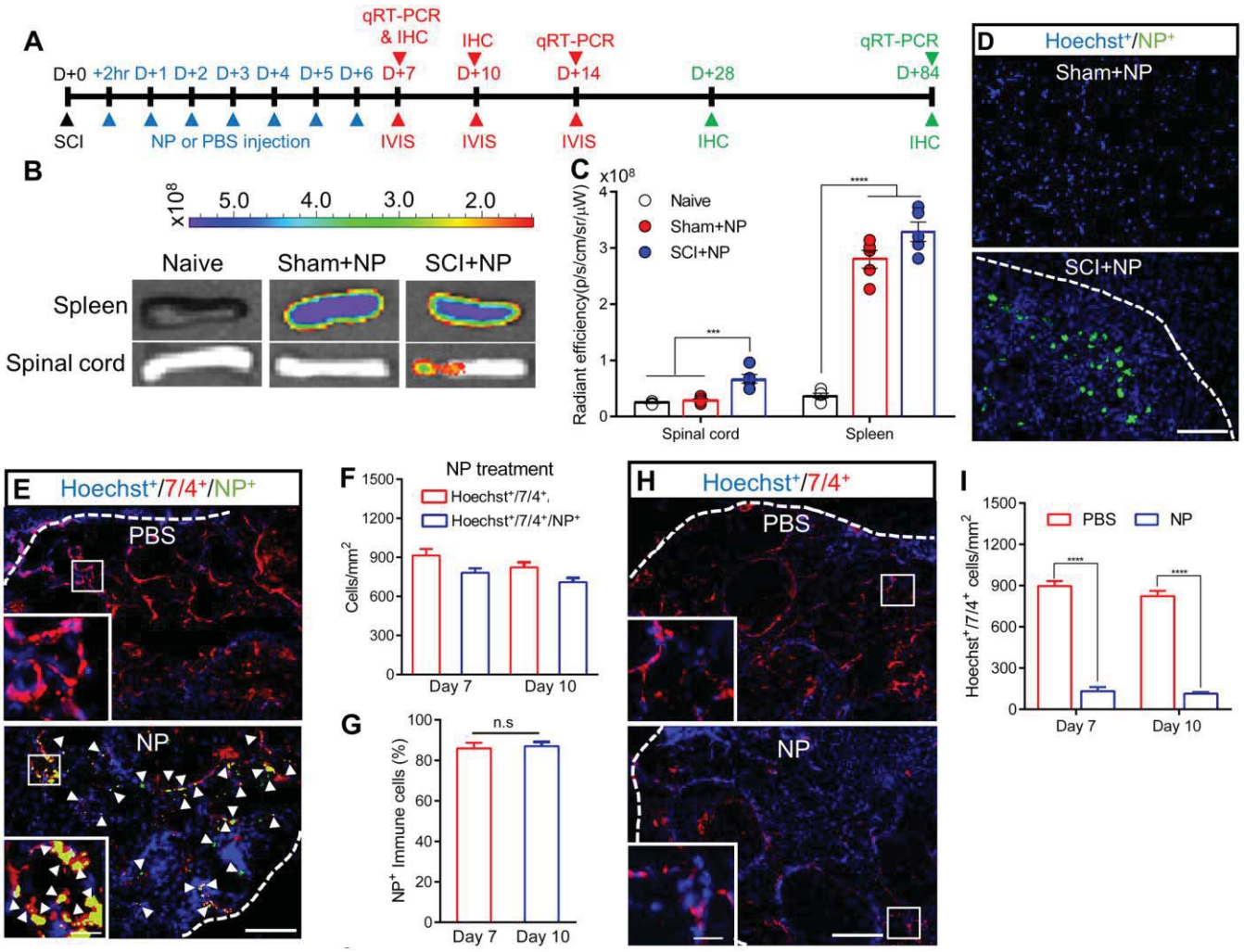

Fig. 1. In vivo biodistribution analysis and internalization of NPs. **(A)** Experimental timeline in this study. **(B)** IVIS images from the spinal cord and spleen were acquired at day 1 post-injection (D+7). **(C)** The fluorescence intensity was quantified in organs from all conditions. **(D)** NPs-Cy5.5 were observed within the injury from SCI group at day 7 post-SCI. The white line indicates implanted bridge area within the spinal cord. **(E)** Spinal cord sections were labelled with anti-7/4 and Hoechst at day 7 post-SCI. NPs-Cy5.5 were colocalized with inflammatory monocytes/neutrophils within SCI in NPs group. Inset: high-magnification image of Hoechst$^+$/7/4$^+$/NP$^+$ within bridge area (yellow and white arrow heads). **(F and G)** The number of Hoechst$^+$/7/4$^+$/NP$^+$ and Hoechst$^+$/7/4$^+$ cells within bridge area from NPs group (F) and percentage of NPs-Cy5.5 expressing immune cells (G) at day 7 and 10 post-SCI. More than 80% of immune cells were colocalized with NPs-Cy5.5 within SCI. **(H)** 7/4$^+$ immune cells distribution from both groups at day 10 post-SCI. **(I)** Number of accumulated immune cells was quantified at day 7 (E) and 10 (H) post-SCI from both conditions. NPs treatment significantly reduced accumulation of immune cells within SCI. A two-way ANOVA with Tukey's post hoc test for the multiple comparisons or unpaired T-test (two-tailed) was performed (G), where ***P<0.001 and ****P<0.0001, mean±SEM, n=5/group. Scale bar: 100 μm

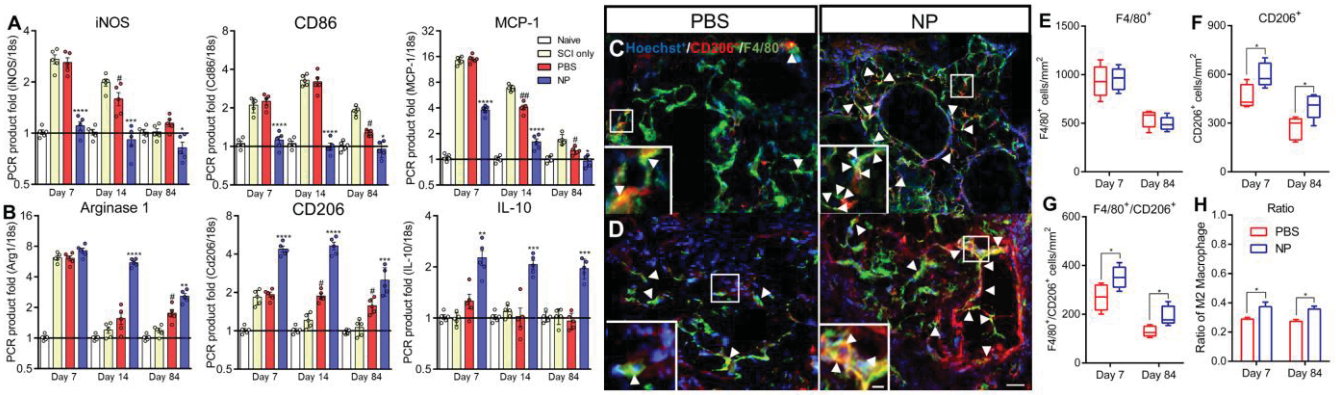

Fig. 2. Immunomodulation and macrophages polarization by NPs. **(A and B)** qRT-PCR data indicate modulation of selected (A) pro-inflammatory and (B) anti-inflammatory markers at day 7, 14, and 84 post-SCI by NPs treatment. A two-way ANOVA with Tukey's post hoc test for the multiple comparisons, where $^{*}P<0.05$, $^{***}P<0.001$ and $^{****}P<0.0001$, compared to PBS group and $^{\#}P<0.05$ relative to SCI only group, mean±SEM, n=5/group and time point. **(C and D)** Immunodetection of M2 ($CD206^{+}/F4/80^{+}/Hoechst^{+}$) macrophages (yellow, white arrow heads, scale bar 100 μm) within bridge from all conditions at day 7 (C) and day 84 post-SCI (D). Inset: high-magnification image of M2 macrophages within bridge area (scale bar: 50 μm). **(E)** The density of total $F4/80^{+}$ macrophages within the bridge. No changes were observed between groups. **(F)** The quantitative analysis of $CD206^{+}$ cells. NPs upregulate the expression of $CD206^{+}$ cells. **(G)** The density of pro-regenerative M2 by NPs. **(H)** The ratio of M2 to the total number of macrophages. A two-way ANOVA with Tukey's post hoc test for the multiple comparisons, where $^{*}P<0.05$, mean±SEM, n=5/group and time point.

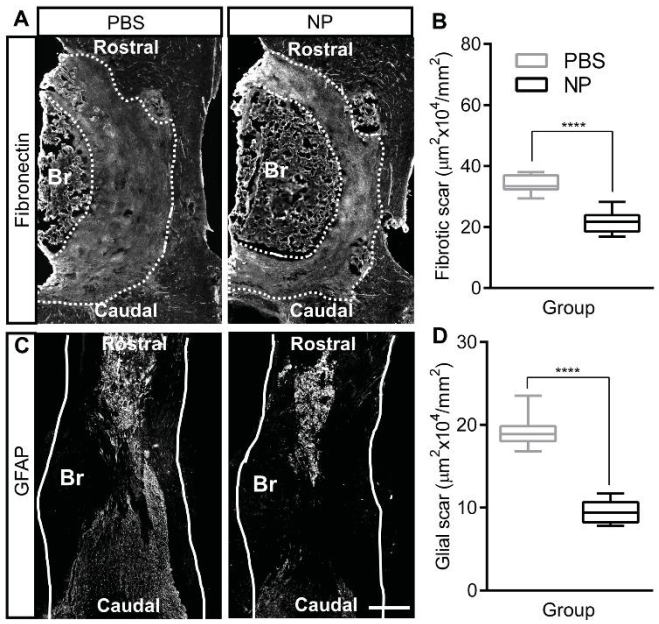

Fig. 3. NPs treatment reduces the fibrotic and gliotic scarring after SCI. **(A and C)** Spinal cord tissues were stained with anti-fibronectin (A) and anti-GFAP (C) using longitudinal sections from 4 weeks after SCI (Br; bridge, dashed line indicates the area of fibrotic scar tissue around bridge and white line indicates host spinal cord, scale bar = 400 μm). **(B and D)** Quantification of fibrotic (B) and glial (D) scarring around implanted bridge area. The area of both fibrotic and glial scar was substantially decreased by NPs treatment. Unpaired T-test (two-tailed) was performed, where $^{****}P<0.0001$, n=5/group.

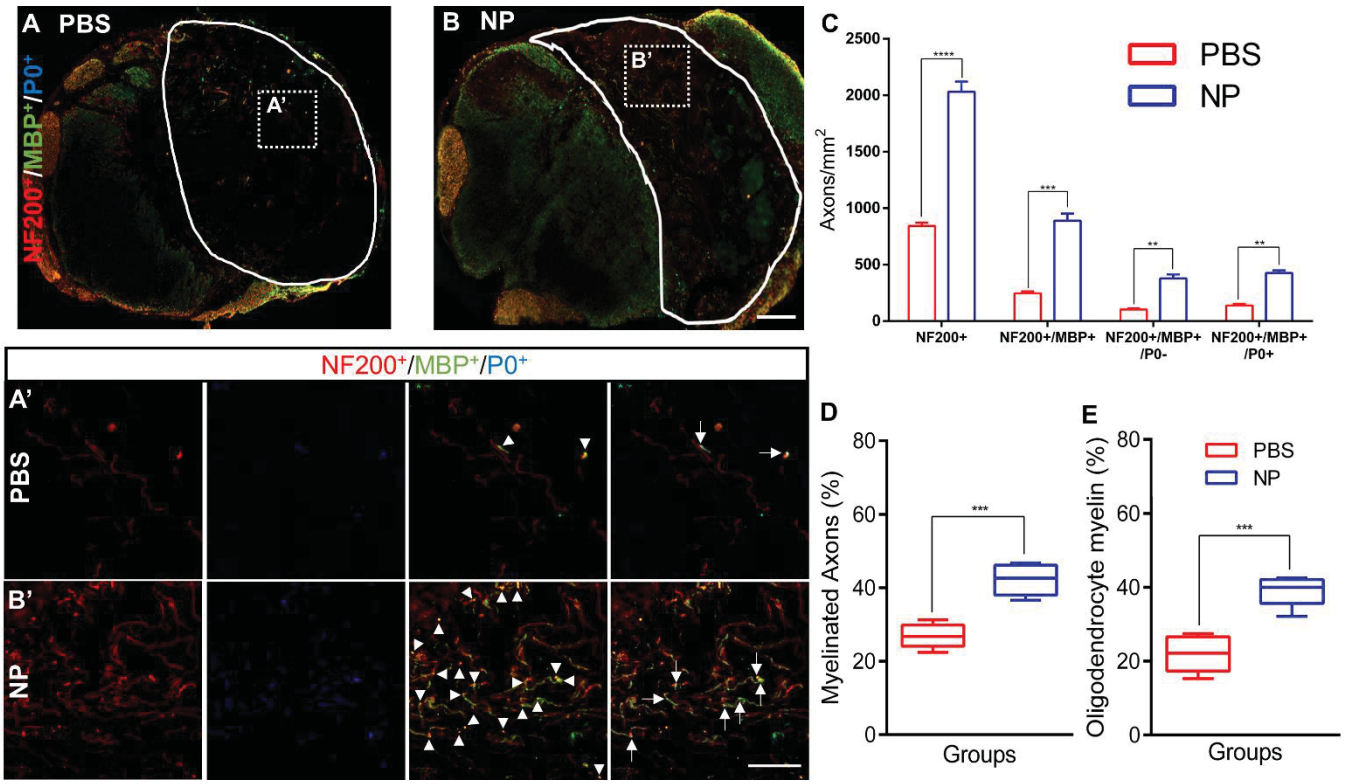

Fig. 4. NPs improve the axonal regrowth and remyelination in the chronic SCI phase. **(A and B)** Spinal cord sections were labelled using NF200 (axons), MBP (all myelination), and P0 (Schwann cells derived myelination) from (A) PBS and (B) NP conditions at the rostral location (scale bar 300 μm). The line indicated the bridge area for quantification and dashed line is for higher magnification area in (A' and B'). White arrowheads show all myelinated axons ($NF200^+/MBP^+$) and white arrows indicate Schwann cell-derived myelinated axons ($NF200^+/MBP^+/P0^+$) (scale bar 100 μm). **(C)** Quantification of total number of $NF200^+$, $NF200^+/MBP^+$, $NF200^+/MBP^+/P0^-$ (oligodendrocyte-mediated myelinated axons), and $NF200^+/MBP^+/P0^+$. **(D)** Proportion of axons that was myelinated within the bridge area. **(E)** Percentage of axons that was myelinated by oligodendrocytes. A two-way (C) ANOVA with Tukey's post hoc test for the multiple comparisons or Unpaired T-test (two-tailed) (D and E) were performed where $^{**}P<0.01$, $^{***}P<0.001$ and $^{****}P<0.0001$, mean±SEM, n=5/group.

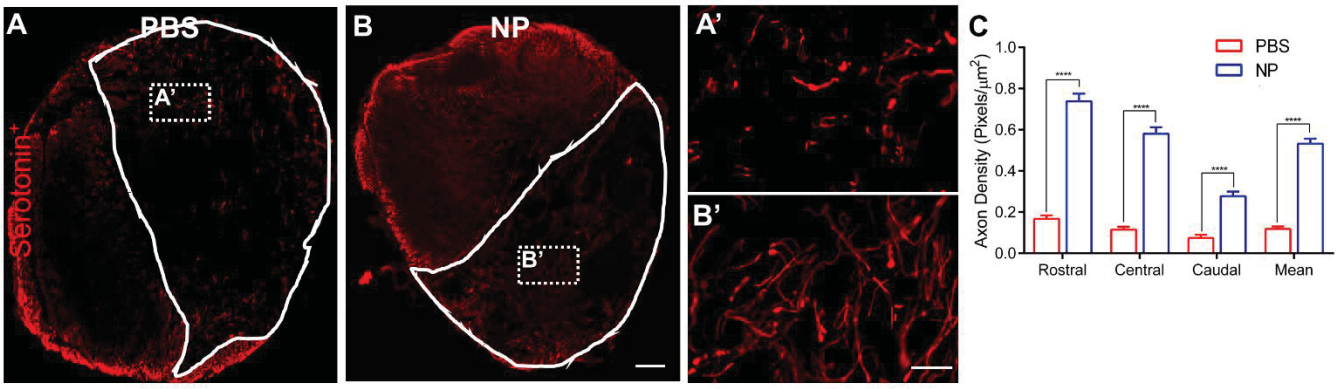

Fig. 5. Density of serotonergic fibers by NPs. **(A and B)** Spinal cord sections were labelled for serotonin from (A) PBS and (B) NPs conditions at the rostral location in the chronic SCI phase (scale bar 300 μm). The line indicated the bridge area for quantification and dashed line is for higher magnification area in (A' and B') (scale bar 100 μm). **(C)** Quantification of serotonergic axonal density in the bridge at rostral (0-400 μm), central (400-800 μm), and caudal (800-1200 μm) locations from the rostral edge of the bridge/tissue interface. A two-way ANOVA with Tukey's post hoc test for the multiple comparisons, where ****P<0.0001, mean±SEM, n=5/group.

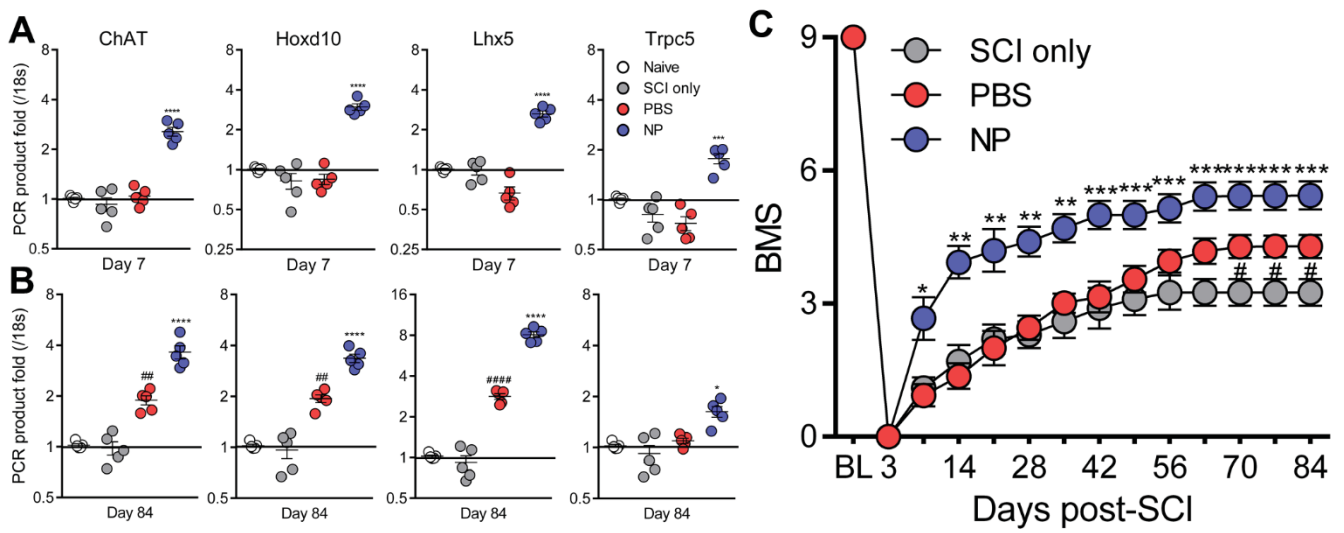

Fig. 6. Locomotor functional recovery by NPs. **(A and B)** Regeneration associated genes were investigated via qRT-PCR in the (A) acute (day 7 post-SCI) and (B) chronic (day 84 post-SCI) SCI phase. NPs injection upregulates levels of regeneration associated gene expression relative to PBS injections. A one-way ANOVA with Tukey's post hoc test for the multiple comparisons, where $^{*}P<0.05$, $^{***}P<0.001$ and $^{****}P<0.0001$ compared to PBS group, $^{\#\#}P<0.01$ and $^{\#\#\#\#}P<0.0001$ relative to SCI only, mean±SEM, n=5/group. **(C)** The ipsilateral hindlimb locomotor function was assessed using the BMS weekly for 84 days after SCI. NPs enhance the locomotor function following SCI. BL; Baseline. A two-way ANOVA with Tukey's post hoc test for the multiple comparisons, where, $^{*}P<0.05$, $^{**}P<0.01$, and $^{***}P<0.001$, compared to PBS group and $^{\#}P<0.05$ relative to SCI only, mean±SEM, n=18/group.

PNAS
www.pnas.org

Supplementary Information for

Intravascular innate immune cells reprogrammed via intravenous nanoparticles to promote functional recovery after spinal cord injury

Jonghyuck Park, Yining Zhang, Eiji Saito, Brian J. Cummings, Aileen J. Anderson, and Lonnie D. Shea

Lonnie D. Shea
Email: ldshea@umich.edu

This PDF file includes:

Supplementary Information Text

SI Materials and Methods

Multichannel bridges fabrication

Initially, PLG (75:25 lactide:glycolide; i.v. 0.76 dL/g; Lakeshore Biomaterials, Birmingham, AL, USA) was dissolved in dichloromethane (6 % w/w) and emulsified in 1% poly(ethylene-alt-maleic anhydride) using a homogenizer (PolyTron 3100; Kinematica AG, Littau, Switzerland) to make microspheres (z-average diameter ~1μm). D-sucrose (Sigma Aldrich), D-glucose (Sigma Aldrich), and dextran MW 100,000 (Sigma Aldrich) were mixed at a ratio of 5.3:2.5:1 respectively by mass then were caramelized, cooled, and drawn from solution using a Pasteur pipette to create sugar fibers. These fibers were coated mixture of PLG microspheres and salt (with a 1:1 ratio), then pressed into a salt-lined aluminum mold. Subsequently, it was equilibrated, and gas formed with high pressure of CO_2 gas (800 psi) for 16 h in a custom-made pressure vessel. The pressure was released over a period of 40 min, which fused adjacent microspheres to produce a continuous polymer structure. The bridges were cut into 1.2 mm sections, and the porogen was leached in water for 2 hours, then the bridges were dried over-night and stored in a desiccator (SI appendix, Fig. S1a).

Nanoparticle fabrication and injection

First, 50:50 Poly(D,L-lactide-co-glycolide) (50:50PLG) (inherent viscosity = 0.55dL/g) was purchased from Absorbable Polymers (Birmingham, AL) , and conjugated with Cyanine 5.5 amine dye (Lumiprobe corporation, Cockeysville, MD) using a N-(3-Dimethylaminopropyl)-N'-ethylcarbodiimide hydrochloride (EDC) (Sigma-Aldrich, St. Louis, MO)/ N-hydroxysuccinimide (NHS) (Thermo Fisher Scientific, Waltham, MA) chemistry. Then, 50:50 PLG particles were fabricated using an oil-in-water single emulsion solvent evaporation method. Briefly, 50:50 PLG polymer and the polymer conjugated with cyanine 5.5 dye were dissolved in dichloromethane. Then, the mixture was added to Poly (ethylene-alt-maleic anhydride) (Polyscience, Inc., Warrington, PA) solution, sonicated using a Cole-Parmer CPX130 Ultrasonic Processor (Vernon Hills, IL), and stirred overnight to remove organic phase. The resulting polymeric particles were washed three times and lyophilized with combination sucrose and D-mannitol (Sigma-Aldrich, St. Louis, MO). For the injections, PLG particles were resuspended in PBS at a concentration of 5 mg/ml and aggregates were removed with a 35 μm mesh filter. Each animal received 1 mg of particles (200 μl of suspension) via tail veil injection within two hours after SCI per day for 7 days. The same volume of PBS was injected as a control.

Spinal cord hemisection injury model and animal care

All animal surgery procedures and animal care were conducted according to the Animal Care and use Committee guideline at University of Michigan. A mouse hemisection SCI model was performed as described previously (1). Briefly, C57/BL6 female mice (6-8 weeks old; The Jackson Laboratory, Bar Harbor, ME, USA) were anesthetized using isoflurane (2%). A dorsal laminectomy was performed at T9-T10 level then a 1.2 mm long lateral of the midline spinal cord segment was cut and removed to generate a hemisection SCI model. Bridges were implanted in the injury site and covered using Gelform (Pfizer, New York, NY, USA) (SI appendix, Fig. S1b). Muscle was sutured together, then the skin was stapled. The animals were placed on a heating pad for recovery. For post-operative animal care, Baytril (enrofloxacin 2.5 mg/kg, once a day for 2 weeks), buprenorphine (0.1 mg/kg, twice a day for 3 days), and lactate ringer

solution (5 mL/100 g, once a day for 5 days) were administrated via subcutaneously. Bladders were manually expressed until bladder reflexive function was observed twice a day.

In vivo bio-distribution of Nanoparticle

For the in vivo biodistribution of NPs study, animals were administered via tail vein with 200 μl of 5mg/ml Cy5.5 conjugated NPs every day for 7 times. 1, 3, and 7 days after injection, animals were euthanized, and tissues were dissected from; spinal cord and spleen. Each tissue was imaged using an IVIS Lumina LTE camera system (Caliper Life Sciences, Hopkinton, MA). The region-of-interest values from each organ were recorded as photon flux in total photon count per cm^2 per steradian.

RNA isolation and Quantitative Reverse-Transcriptase PCR

Initially, the spinal cord tissues were removed from all conditions. The spinal cord tissues were removed and cut into about 2 mm segments centered on 1.2 mm of bridge region; samples were not pooled. Next, samples were homogenized using 1 ml of Trizol reagent (Invitrogen, Carlsbad, CA) with a glass tissue grinder. Samples were not pooled. RNA isolation was followed by chloroform extraction and isopropanol precipitation (2). The concentration of RNA was measured using NanoDrop 2000C (Thermo Scientific, Newark, DE). Next, we conducted the quantitative Reverse-Transcriptase PCR (qRT-PCR) using spinal cord for the gene expression analysis over time. cDNA was synthesized using iScript™ cDNA Synthesis kit (Bio-Rad, Hercules, CA). Primers were designed for qRT-PCR (SI appendix, Table. S1) (1, 3, 4). The qRT-PCR products were assessed using the accumulation level of iQ™ SYBR Green Supermix (Bio-Rad) fluorescence following a manufacturer's protocol on CFX Connect™ Real-Time PCR Detection System (Bio-Rad). The gene expression level was normalized by the expression of 18s-rRNA and differences in gene expression were presented as fold ratios from control group. Relative quantification was calculated as $X = 2^{-\Delta\Delta Ct}$, where $\Delta\Delta C_t = \Delta E - \Delta C_t$ and $\Delta E = C_{t,exp} - C_{t,18s\text{-}rRNA}$, $\Delta C_t = C_{t,\ control} - C_{t,18s\text{-}rRNA}$ (5). All qRT-PCR values were expressed as the log2 transformed after normalization to the housekeeping gene 18s-rRNA and +1 was marked as cut-off value for upregulation.

Behavioral test for locomotor function

Locomotor functional recovery in the ipsilateral hindlimb after SCI was accessed using open field Basso Mouse Scale (BMS) locomotor rating scale with a score from 0 (no movement) to 9 (normal gait) (6). The score is based on the ipsilateral hindlimb locomotor ability of SCI mice. SCI mice (n=18/group) were observed in an open field for 4 minutes after they had gently adapted to the field. Only the ipsilateral hindlimb side was assessed at days 3 and then weekly after SCI for 12 weeks. The score was obtained by taking an average value of results from each experimental group. A baseline (BL) was determined at day 7 and 1 prior to the SCI. Animals were randomly assigned to treatment group and assessment was performed by researchers blinded to the group.

Tissue processing and immunofluorescence

Spinal cord tissues were collected at 1, 4, and 12 weeks after SCI. Those tissues were then snap frozen in isopentane and embedded in Tissue Tek O.C.T compound (Sakura Finetek, Torrance, CA, USA) with 30% sucrose. Samples were cryosectioned in

18 μm transversely or in 12 μm longitudinally. The following antibodies were used for immunofluorescence: anti-Mannose receptor (anti-CD206, 1:200, ab195192, Abcam, Cambridge, MA), F4/80 (1:200, MCA497GA, AbD Serotec, Raleigh, NC), 7/4 (1:200, MCA771GA, Bio-Rad), Neurofilament 200 (NF200, 1:200, Sigma Aldrich, St. Louis, MO), Myelin Basic Protein (MBP, 1:500, Santa Cruz Biotech, Dallas, TX), P-zero myelin protein (P0) (1:250, Aves Labs, Tigard, OR), anti-fibronectin (1:200, F7387, Sigma), anti-GFAP (1:500, ab53554, Abcam), anti-serotonin (1:400, ab66047, Abcam) and Hoechst 33258 for counterstain (1:2000, H3569, Fisher Scientific, Hampton, NH). Species-specific secondary antibodies were used for the detection (1:1000, Fisher Scientific, unless otherwise noted); AlexaFluor 555 goat anti-rabbit IgG (A-21429), AlexaFluor 555 goat anti-mouse IgG (A-21424), AlexaFluor 488 donkey anti-goat IgG (A-11055), AlexaFluor 555 donkey anti-goat IgG (A-21432), AlexaFluor 647 donkey anti-goat IgG (A-21447), AlexaFluor 647 donkey anti-mouse IgG (A-31571). The number of immune-positive cells were manually counted and done under blinded conditions. Multiple markers by co-staining was examined by evaluating pixel overlap of different channels in NIH ImageJ (Bethesda, MD, USA). Nonadjacent nine spinal cord tissues were selected randomly from three distinct locations at caudal (0-400 μm), central (400-800 μm), and rostral (800-1200 μm) from the caudal edge of the bridge/tissue interface (total 27 tissues were assessed per animal) (SI appendix, Fig. S1C). The accumulated inflammatory monocytes/neutrophils within a bridge were identified by co-labelling Hoechst$^+$ to 7/4 immunoreactive cells from day 7 and 10 following SCI. The percentage of 7/4$^+$ inflammatory monocytes/neutrophils that was co-labeled with NPs-Cy5.5 was determined from the ratio of the number of Hoechst$^+$/7/4$^+$/NP$^+$ cells divided by the number of Hoechst$^+$/7/4$^+$ cells within the bridge area. The total number of macrophages and pro-regenerative M2 macrophages within a bridge area were evaluated by determining Hoechst$^+$/F4/80$^+$ cells and Hoechst$^+$/F4/80$^+$/CD206$^+$ cells. Macrophages were identified by localizing Hoechst$^+$ staining to F4/80$^+$ immunoreactive and labeling them in ImageJ. Then, cell numbers were normalized to the counted area in each tissue section. To investigate the numbers of regenerated and myelinated neurofilaments, we used NF200$^+$, NF200$^+$/MBP$^+$, and NF200$^+$/MBP$^+$/P0$^+$ axonal fibers to identify the numbers of axons, all myelinated axons, and myelinated axons by infiltrating Schwann cells, respectively. The percentage of myelinated axons was determined from the ratio of the number of myelinated axons (NF200$^+$/MBP$^+$) divided by the number of axons (NF200$^+$) within the bridge area. To determine the source of the myelination, we performed triple staining of NF200, MBP and P0. NF200$^+$/MBP$^+$/P0$^-$ neurofilaments were considered as oligodendrocyte-derived myelination. The fraction of oligodendrocyte-derived myelination was calculated as NF200$^+$/MBP$^+$/P0$^-$ divided by NF200$^+$/MBP$^+$. To evaluate fibrotic and glial scarring area around implanted multichannel bridges, nine nonadjacent sagittal sections were selected randomly from each animal and condition, and the area of fibrotic and gliotic scarring around the implanted bridge was investigated. The immunofluorescence images were converted to black and white then a standardized optical density threshold to each image was applied. ImageJ was used to measure the amount of stained area around the implanted bridges. To investigate the intensity of serotonergic fibers, total labelled pixels of serotonin labeled axons within the bridge area were quantified and divided by the bridge area to obtained mean serotonergic axon density. All Tissues were imaged on an Axio Observer Z1 (Zesis, Oberkochen, Germany) using a 10x or 20x/0.45 M27 apochromatic objective and an ORCA-Flash 4.0 V2 Digital CMOS camera (C11440-22CU, Hamamatsu Photonics, Hamamatsu City, Shizuoka, Japan).

Statistical analysis

A one or two-way ANOVA and Tukey's post hoc test for the multiple comparisons, and Student's t test were used for the statistical analysis. To achieve reasonable statistical power analyses, type II errors were controlled at 0.2 level for all the statistical tests and α=0.05. Equal variance (ANOVA Model) was validated and assumed for each study. Given the above parameters, a conservative effect size was 0.25 for appropriate sample size for each study and all statistical analysis were performed using G* Power Software (1), OriginPro (OriginLab Corporation, Northampton, MA, USA), and Prism 6 (GraphPad Software, La Jolla, CA, USA). $P<0.05$ was considered as statistically significant and the all values were expressed in mean$\pm$ standard error of mean (SEM).

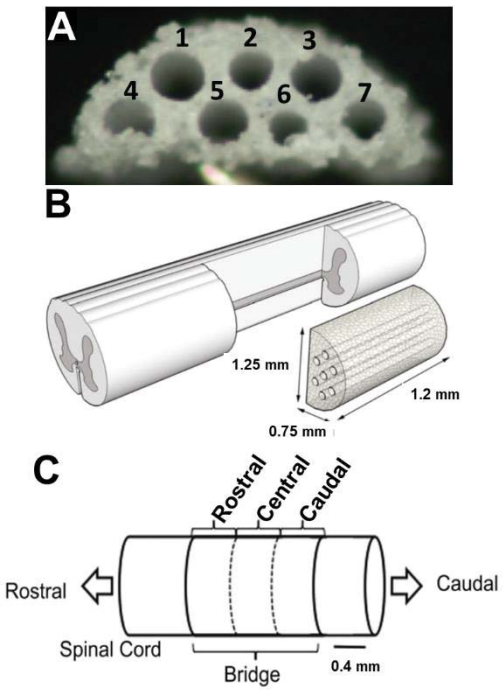

Fig. S1. PLG multichannel bridge and hemi-sectional SCI model. **(A)** Photomicrograph of a bridge with 200 μm multichannel. **(B)** Schematic representation of hemi-section SCI at T9-T10 and multichannel bridge implantation Illustrating approximate bridge dimensions. **(C)** Schematic multichannel bridge regions where the bridge was divided for analysis. From the rostral edge of the bridge/tissue interface, rostral region analysis was done at 0-400 μm, central at 400-800 μm, and caudal at 800-1200 μm.

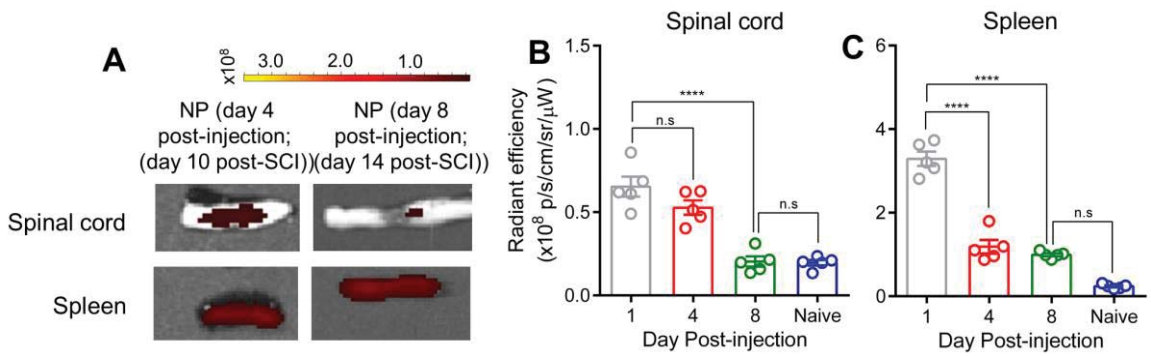

Fig. S2. In vivo biodistribution of NPs over time. **(A)** The spinal cord and spleen were collected from SCI with NPs treatment group at day 4 and 8 post-injection and IVIS images were acquired. **(B)** The fluorescence intensity was quantified in organs as a function of time. A two-way ANOVA with Tukey's post hoc test for the multiple comparisons, where $^{****}P<0.0001$, mean±SEM, n=5/group.

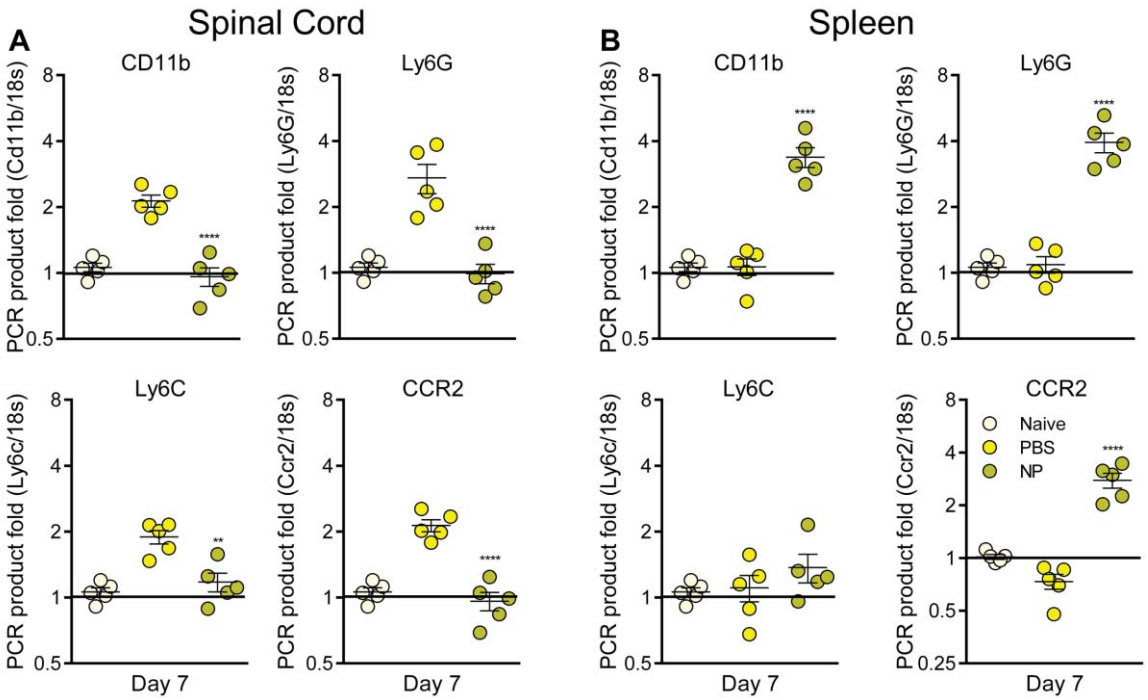

Fig. S3. Gene expression of neutrophils markers Cd11b and Ly6G and inflammatory monocytes markers Ly6c and Ccr2 were investigated from **(A)** spinal cord and **(B)** spleen through qRT-PCR at day 7 post-SCI in all conditions. The data suggest that NP-Cy5.5 downregulate the levels of neutrophils and inflammatory monocytes at the injured area. A one-way ANOVA with Tukey's post hoc test for the multiple comparisons, where $^{**}P<0.01$, and $^{****}P<0.0001$, mean±SEM, n=5/group.

Table S1. Primer sequence for qRT-PCR

Gene	Accession number	Forward (5'-3')	Reverse (5'-3')
Arginase1	U51805.1	GAACACGGCAGTGGCTTTAAC	TGCTTAGCTCTGTCTGCTTTGC
CD206	NM_008625.2	TCTTTGCCTTTCCCAGTCTCC	TGACACCCAGCGGAATTTC
IL-10	NM_010548.2	ATGCAGGACTTTAAGGGTTACTTGG GTT	ATTCGGAGAGAGAGGTACAAACGAGG TTT
iNOS	U58677.1	CCCTTCAATGGTTGGTACATGG	ACATTGATCTCCGTGACAGCC
Cd86	NM_019388.3	TTGTGTGTGTTCTGGAAACGGAG	AACTTAGAGGCTGTGTTGCTGGG
MCP-1	NM_011333.3	GCCAACTCTCACTGAAGCCA	TGCTGCTGGTGATCCTCTTG
Chat	NM_009891.2	GGCTTTTGTGCAAGCCATGA	CACAGGGCCATAACAGCAGA
Hoxd10	NM_010462.5	TGTACAGTGCAGAGAAGCGG	GTGTCTGGACTGGAGTCTGC
Lhx5	NM_008499.5	CAGGATCCGTTACAGGACGA	AACCACACCTGAATGACCCT
Trpc5	NM_009428.3	AACTCCCTCTACCTGGCAAC	TTCTGCAATCAGAGTCGGGT
18s-rRNA	NR_003278.3	GCAATTATTCCCCATGAACG	GGCCTCACTAAACCATCCAA
Cd11b	NM_008401.2	AAGCAGCTGAATGGGAGGAC	TAGATGCGATGGTGTCGAGC
Ly6G	NM_001310438.1	GAGCAATCTCTGCCTTCCCA	AGGAGTGGGGTGCCTATACA
Ccr2	NM_009915.2	AACAGTGCCCAGTTTTCTATAGG	CGAGACCTCTTGCTCCCCA
Ly6c	NM_001252057.1	GACAGAACTTGCCACTGTGC	GCTGGGCAGGAAGTCTCAAT

References

1. Park J*, et al.* (2018) Local Immunomodulation with Anti-inflammatory Cytokine-Encoding Lentivirus Enhances Functional Recovery after Spinal Cord Injury. *Mol Ther* 26(7):1756-1770.
2. Park J*, et al.* (2015) Acrolein contributes to TRPA1 up-regulation in peripheral and central sensory hypersensitivity following spinal cord injury. *J Neurochem* 135(5):987-997.
3. Due MR*, et al.* (2014) Acrolein involvement in sensory and behavioral hypersensitivity following spinal cord injury in the rat. *J Neurochem* 128(5):776-786.
4. Chen Z*, et al.* (2016) Mitigation of sensory and motor deficits by acrolein scavenger phenelzine in a rat model of spinal cord contusive injury. *Journal of Neurochemistry* 138(2):328-338.
5. Livak KJ & Schmittgen TD (2001) Analysis of relative gene expression data using real-time quantitative PCR and the 2(T)(-Delta Delta C) method. *Methods* 25(4):402-408.
6. Basso DM*, et al.* (2006) Basso Mouse Scale for locomotion detects differences in recovery after spinal cord injury in five common mouse strains. *J Neurotrauma* 23(5):635-659.
7. Pineau I, Sun L, Bastien D, & Lacroix S (2010) Astrocytes initiate inflammation in the injured mouse spinal cord by promoting the entry of neutrophils and inflammatory monocytes in an IL-1 receptor/MyD88-dependent fashion. *Brain Behav Immun* 24(4):540-553.
8. Tsou CL*, et al.* (2007) Critical roles for CCR2 and MCP-3 in monocyte mobilization from bone marrow and recruitment to inflammatory sites. *J Clin Invest* 117(4):902-909.